Front dynamics of pH oscillators with initially separated reactants

Brigitta Dúzs[†], István Szalai[‡]

[†] Institute of Chemistry, Laboratory of Nonlinear Chemical Dynamics, Eötvös University, Pázmány Péter sétány 1/A, Budapest 1117, Hungary, orcid.org/0000-0002-0909-2808

[‡] Institute of Chemistry, Laboratory of Nonlinear Chemical Dynamics, Eötvös University, Pázmány Péter sétány 1/A, Budapest 1117, Hungary, email: pisti@chem.elte.hu, phone number: +36-1-372-2500/1902, orcid.org/0000-0002-1859-1043

Abstract

The spatiotemporal dynamics of the Landolt-type pH oscillators are studied both numerically and experimentally with initially separated reagents in space. This configuration results in an A + B → oscillator front type system with localized patterns. The generic Rábai model of the pH-oscillators predicts the formation of an asymmetric acidic domain at the interface of the two zones loaded by different sets of chemicals. This asymmetry is rather caused by the initial conditions than the difference in the diffusivities of the components. As the influence of the negative feedback process increases, this acidic zone becomes to be localized around the interface. At some point the acidic zone bifurcates, a less acidic zone separates and starts to move forward the oxidant rich zone. In a limited domain of parameters, spatiotemporal oscillations are found due to the instability of the main acidic zone. The appropriate conditions for the development of this periodic behaviour is characterized by simulations. The numerically predicted phenomena are supported by experiments performed with the bromate-sulfite-ferrocyanide and with the hydrogen peroxide-sulfite-ferrocyanide systems, except the oscillatory phenomena.

Keywords

Introduction

Out-of-equilibrium chemical reaction-diffusion systems are capable to produce a large variety of self-organized dissipative structures, such as traveling fronts, waves and stationary patterns. These structures can form either in conditions where the initial reactants are homogeneously distributed or in the presence of gradients in the concentrations of the initial reactants.

The classical examples of the first type are the wave patterns develop in the initially well mixed solution of the Belousov-Zhabotinsky (BZ) reaction in a petri-dish [1]. These phenomena form in such a simple setup, because the BZ reaction belongs to a special class of the oscillatory reactions, which can produce transient dynamical phenomena (e.g. oscillations, waves) under batch conditions. The species which play important role in the dynamics of this type of reactions, are intermediates and not initial reagents. Thus, the initial reagents, which are consumed relatively slowly, act as homogeneous sources of the dynamical species. The situation is quite different in those reactions, where the initial reagents are directly involved in the main dynamical processes. In this case, to prepare a starting homogeneous mixture, the reaction must have an induction period that is longer than the time scale of the mixing. Well-known examples of these systems are the autocatalytic reactions, e.g. the chlorite-tetrathionate (CT) reaction, which can produce planar and cellular fronts after mixing the initial reactants [2].

The dynamics of the systems which are imposed by gradients are essentially different from the ones which start from a homogeneous state. The presence of gradients in the concentrations of the initial reactants broadens the range of the chemical reactions, which can be used to study non-trivial reaction-diffusion patterns. Simple precipitation reactions with initially separated reagents are ready to form Liesegang-patterns or chemical gardens, the two well-known examples of chemical self-organization [3,4]. Here, the reactions, which might have relatively simple kinetics with a short time-scale, are coupled to the counter-diffusion of the initial reagents and to heterogeneous processes.

In their pioneering theoretical work, Gálfi and Rácz described the properties of fronts appear in the presence of gradients in the concentrations of the initial reactants [5]. They have found that the centre and the width of the front scale with time as $t^{1/2}$ and $t^{1/6}$ in case of a second order A + B $\rightarrow$ C reaction, when the two reactants are initially separated in space. The properties of such kind of fronts have been analysed in details during the past decades. Recently, the group of Anne De Wit have investigated theoretically and experimentally the dynamics of an A + B $\rightarrow$ oscillator front, where the initial reactants of an oscillatory reaction are separated in space at the beginning [6-8]. Their theoretical results show diverse spatially localized dynamics, including the formation of localized waves and Turing patterns. In the experiments, they used the BZ reaction to provide oscillatory chemistry and they have observed the predicted wave phenomenon.

Here we present a numerical and experimental investigation on the dynamics of an A + B $\rightarrow$ oscillator type front using pH-oscillators, when the reactants are separated initially in space. Contrary to the BZ reaction, the pH oscillators do not show periodic behaviour under batch conditions. These reactions are capable to generate large amplitude sustained pH-oscillations only in a continuously-fed stirred tank reactor (CSTR) and transient periodic behaviour in a semi-batch or a gel-fed reactor [9]. The

3

reaction-diffusion dynamics of pH-oscillators have been explored in open one-side-fed reactors, where the feed of the initial reagents is made from one surface of the reaction medium, which is often a hydrogel. This design provides a feed of fresh reactants from the same direction and allow to maintain fixed concentrations at the feeding boundary. The reactants diffuse in to the reaction medium, where the reaction-diffusion patterns may appear. In this configuration, the time-scale of the diffusive fed is an important factor of the dynamics. The use of the one-side-fed-reactors has made possible to produce special patterns with the type of the oscillatory reactions, which requires a continuous supply of the initial reagents to work. As a result, propagating fronts, chemical waves, different types of stationary patterns have been observed experimentally in many different reactions during the past years [10].
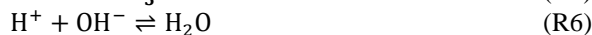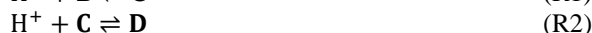
In this work, we apply Landolt-type pH-oscillators, which are based on the acid catalysed oxidation of a reductant (e.g. sulfite ions) by an oxidant (e.g. iodate, bromate, or hydrogen peroxide) and supplemented with a proton consuming reaction. This latter process can be actualized by a reaction between the oxidant and a second reductant (e.g. ferrocyanide, thiosulfate, or thiourea) or by using an appropriate protonation equilibrium (e.g. hydrogen carbonate/carbonic acid). Contrary to the BZ reaction, in pH-oscillators the initial reagents are directly involved in the positive and negative feedback processes, and they do not show oscillations in a batch reactor. The advantages of these systems are their variable chemistry, which provides a flexibility for the experiments, and the availability of a simple skeleton model, which can be used for the simulations.

In this work, we initiate a front by putting two gels, containing the main reactants of the pH-oscillators, in contact. The reaction starts at the interface between these gels. As the reactants diffuse toward each other, they can react and form an autocatalytic front, and even spatio-temporal oscillations under appropriate conditions. We first give a numerical exploration using a mathematical model based on the Rábai-model of the pH-oscillators [11]. Experimental observations are also presented and compared with the theoretical results.

Numerical study

Model and method

The general model of Landolt-type pH oscillators proposed by Rábai [11] provides a simple and efficient way to reproduce the experimental findings of these chemical systems even in batch or under continuously fed conditions [12]. To be consequent we use the following form of the Rábai model:

$$H^+ + \mathbf{B} \rightleftharpoons \mathbf{C} \tag{R1}$$
$$H^+ + \mathbf{C} \rightleftharpoons \mathbf{D} \tag{R2}$$
$$\mathbf{C} + \mathbf{Ox} \rightarrow H^+ + \mathbf{P_1} \tag{R3}$$
$$\mathbf{D} + \mathbf{Ox} \rightarrow 2H^+ + \mathbf{P_2} \tag{R4}$$
$$H^+ + \mathbf{Y} \rightarrow \mathbf{P_3} \tag{R5}$$
$$H^+ + OH^- \rightleftharpoons H_2O \tag{R6}$$

where $\mathbf{B}$, $\mathbf{C}$ and $\mathbf{D}$ are differently protonated forms of the substrate (e.g. SO_3^{2-}, HSO_3^- and H_2SO_3, respectively), $\mathbf{Ox}$ is the oxidant (e.g. H_2O_2, BrO_3^-, IO_3^-), $\mathbf{Y}$ is a H^+-consuming species and $\mathbf{P_1}$, $\mathbf{P_2}$ and $\mathbf{P_3}$ are products.

$$r_1 = k_1[H^+][\mathbf{B}] - k_{1b}[\mathbf{C}] \tag{1}$$
$$r_2 = k_2[H^+][\mathbf{C}] - k_{2b}[\mathbf{D}] \tag{2}$$
$$r_3 = k_3[\mathbf{C}][\mathbf{Ox}] \tag{3}$$
$$r_4 = k_4[\mathbf{D}][\mathbf{Ox}] \tag{4}$$
$$r_5 = k_5[H^+][\mathbf{Y}] \tag{5}$$
$$r_6 = k_6[H^+][OH^-] - k_{6b} \tag{6}$$

where [ ] stands for molar concentrations, k_n are reaction rate constants. The first two steps are the protonation equilibrium of the substrate (R1-R2). The doubly protonated form ($\mathbf{D}$) reacts more rapidly with the oxidant than the simple protonated one ($\mathbf{C}$), as k_4 is typically several orders of magnitude larger than k_3. The first four steps together (R1-R4) can be referred as the autocatalytic oxidation of the substrate, where H^+ is the autocatalytically produced component. The additional H^+-consuming process is accounted by (R5) [10]. If not indicated differently, calculations are carried out with the parameters presented in Table 1. These data correspond to the hydrogen peroxide-sulfite-ferrocyanide system.

Table 1 Rate constants and diffusion coefficients used in the calculations

rate constants		ref.	components	$D_i \times 10^{-5}$ / cm^{2}s^{-1}	ref.
k_1 / M^{-1}s^{-1}	5×10^{10}	[13]	H^+	9.3	[14]
k_{1b} / s^{-1}	3×10^3	[13]	B	1.1	[14]
k_2 / M^{-1}s^{-1}	2×10^8	[13]	C	1.5	[14]
k_{2b} / s^{-1}	3.4×10^6	[13]	D	1.6	[13]
k_3 / M^{-1}s^{-1}	7.01	estimated	Ox	1.5	[15]
k_4 / M^{-1}s^{-1}	2.66×10^5	values	Y	0.7	[14]
k_5 / M^{-1}s^{-1}	200	[10]	OH$^-$	5.26	[14]
k_6 / M^{-1}s^{-1}	1×10^{11}	[13]			
k_{6b} / Ms^{-1}	1×10^{-3}	[13]			

Here we present one-dimensional reaction-diffusion simulations along axis x. As indicated in Fig. 1, this direction is parallel with the direction of the initial concentration gradients. The two halves are called according to the initial concentration distribution. Each of the halves are filled homogeneously at the beginning but they differ in the initial chemical composition: the OX part contains **Ox**, the ACID part contains H^+ and both parts contain equal amount of **B** and equal amount of **Y**. The applied reaction-diffusion equation set is the following:

$$\partial_t \mathbf{c} = \mathbf{f}(\mathbf{c}, k_1, \ldots, k_n) + \mathbf{D}\partial_x^2 \mathbf{c} \tag{7}$$

where **c** is the vector of the molar concentrations, **f** represents the chemical kinetic functions, and **D** is the diagonal matrix of the diffusion coefficients. Neumann boundary conditions were applied at the first and the last gel points, which results in continuously changing concentrations in time at the boundaries. In this initially separated configuration, the reaction zone evolves at the cross-gradients of the reactants. The partial differential equations were discretized with a standard second-order finite difference scheme on 800 mesh. The resulting system were solved by the SUNDIALS CVODE [16] solver using backward differentiation formula method. The absolute and relative error tolerances were 10^{-10} and 10^{-8}, respectively.
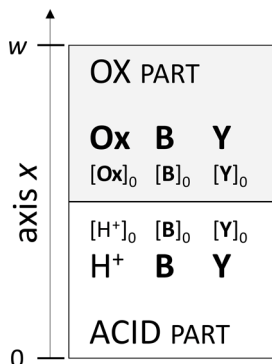

Fig. 1 The sketch of the investigated setup with the initial concentration distribution of the reactants. The parts are named after the main components which are initially separated. The initial concentrations of **B** and **Y** are equal in both parts. The axis of the one-dimensional simulations is denoted by x, and the width of the one-dimensional system is w

Results

We start with the dynamical behaviour of the model *in the absence* of the H^+-consumer **Y** component. Fig. 2a presents a typical time-space plot of this case. During the first period ($t = 0 - 45$ s) there is no sharp change in the pH, but the counter-diffusion has already brought together the initially separated components. Looking at the concentration profiles at $t = 30$ s (Fig. 2b) there is a minimum in [**B**] at $x = 0.8$ cm, which confirms that the (R3-R4) autocatalytic process starts before $t = 45$ s.
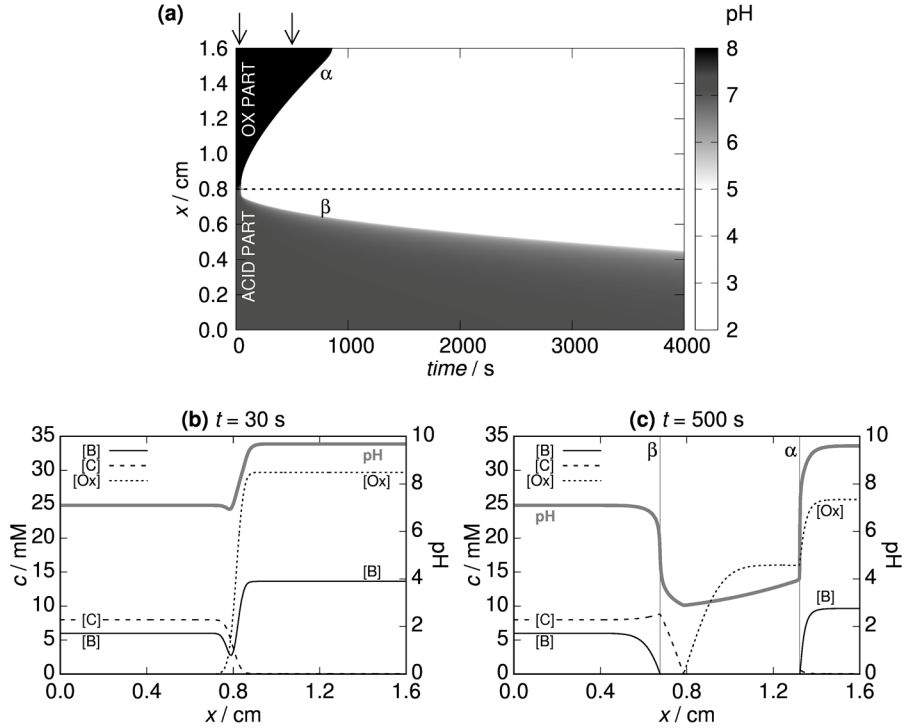
Fig. 2 Calculated spatiotemporal evolution of the pH and the molar concentrations in the absence of **Y**. (a) Time-space plot of the pH. The light colour represents the acidic region. The arrows indicate the times of the concentration profiles. (b)-(c) Spatial profiles at (b) $t = 30$ s and (c) $t = 500$ s. Initial concentrations: $[\mathbf{Ox}]_{0,OX} = 0.030$ M, $[\mathbf{H}^+]_{0,ACID} = 0.008$ M, $[\mathbf{B}]_{0,both} = 0.014$ M, $w = 1.6$ cm

From $t = 45$ s an acidic band appears in the time-space plot (Fig. 2a), which corresponds to the appearance of a front pair (α and β). The spatial front positions are defined as the maximums of the derivatives of the $[\mathbf{B}](x)$ curves, which are coincide with the maximums of the derivatives of the pH(x) curves in both sides in the absence of **Y**. *Front α* propagates towards the OX side and β towards the ACID side. At the position of α the pH step is between 3.8 and 9.8, at the position of β the pH step is between 3.0 and 7.0 (see Fig. 2c) and these steps remain constant in time. The width of the band grows as these fronts propagate along x. In this asymmetric concentration distribution, the fronts are expected to behave differently. The autocatalytic front indicated by α moves quickly through the OX part, because at that region the main components of the autocatalytic process (**Ox** and **B**) are both present in a sufficient amount. The propagation of α ends when the substrate is consumed on the OX side.

The initial $[\mathbf{Ox}]_0$ is in excess compared to $[\mathbf{B}]_0$, so there is a considerable amount of **Ox** between α and β as well. In this region, the autocatalytic process is slower than at the position of α, due to the lack of the substrate and the decreasing amount of the oxidant. At $x = 0.78$ cm, which is a fix position in time, both **C** and **Ox** are used up in the slow autocatalytic process, so this position can be considered as the border of the autocatalytic region. Therefore, *front β* is the consequence of the spatial distribution

7

of **B** and **C**, and moves according to the accumulating H$^+$ coming from the direction of *front* α.

The asymmetric nature of α and β fronts are demonstrated in Fig. 3. The decrease of the initial concentration of the oxidant results in the reversal of the propagation of *front* β, and now it also propagates to the direction of the OX part. According to our simulations, the direction of the propagation of β can be tuned by the initial [**B**]$_0$ / [**Ox**]$_0$ ratio.
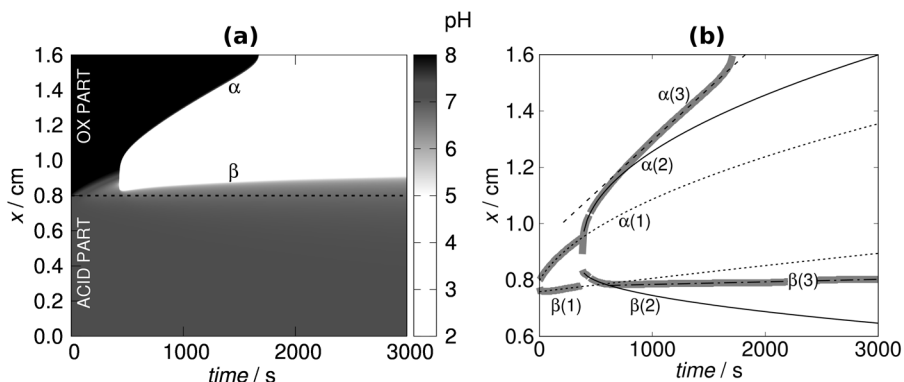

Fig. 3 The reverse propagation of front β in a calculated time-space plot of the pH in the absence of **Y** (a) and the detailed analysis of the fronts of the same case (b). In (a) the light colour represents the acidic region. In (b) the α(1-3) and β(1-3) signs refer to the different parts of the fronts. The dotted, solid and dash-dot lines correspond to fittings with a function $f(t) = p_0 + p_1 \times t^{1/2}$, and the dashed line corresponds to the fitting of a linear function of time. Initial concentrations: [**Ox**]$_{0,OX}$ = 0.016 M, [H$^+$]$_{0,ACID}$ = 0.008 M, [**B**]$_{0,both}$ = 0.014 M, w = 1.6 cm

The temporal propagation of the fronts provides information about the nature of the undergoing processes. In Fig. 3b we show the typical time evolution of *front* α and β which can be separated into three parts. Before the appearance of the middle acidic zone, both α(1) and β(1) scale with time as $t^{1/2}$ as the process is diffusion limited. The second part starts at the outbreak of the free H$^+$ ions. Then a new diffusion limited front sections develop, which propagate significantly faster than α(1) and β(1). In the third part, the autocatalytic process becomes dominant in case of *front* α and this results in a constant velocity of α(3). We found a square root dependence of this velocity on the initial concentrations of H$^+$ and **Ox** and a reciprocal of initial concentration of **B**.

$$v_{\alpha(3)} \propto [\text{H}^+]_0^{1/2}[\textbf{Ox}]_0^{1/2}[\textbf{B}]_0^{-1/2} \tag{8}$$

This result is in a good agreement with the fact that **B** is an inhibitor of the autocatalytic process and consistent with the substrate inhibition mechanism suggested by Rábai [11]. The direction of propagation of β(3) is determined by the presence of the two opposite tendencies of β(1) and β(2).

In the next step, we investigate the phenomena in the presence of **Y**. Fig. 4 shows the time-space plot of this case: the main acidic band in the middle is quite narrow compared to the previous situation, and a new phenomenon, a narrow acidic arch appears in the OX part. The width of the main band remains almost constant, as it can be seen by comparing Fig. 4b and Fig. 4c. The whole band propagates slowly along

coordinate x according to the gradients of [**C**] and [**Ox**], which is similar to what we presented above for *front β*. The maximum pH of the main band is around pH = 5 and the dominant H^+ producing reaction is (R4). In contrast, at the region of the acidic arch the pH is around pH = 7, and the overall reaction rate of the autocatalytic process is slower.
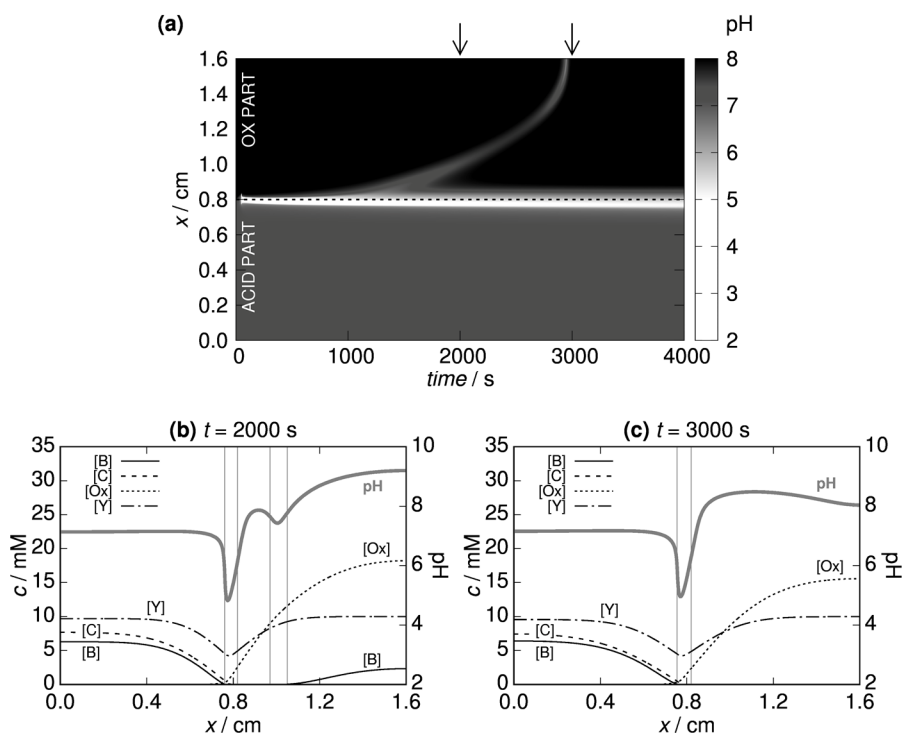

Fig. 4 Calculated spatiotemporal evolution of the pH and the molar concentrations in the presence of **Y**. (a) Time-space plot of the pH. The light colour represents the acidic region. The arrows indicate the times of the concentration profiles. (b)-(c) Spatial profiles at (b) $t = 2000$ s and (c) $t = 3000$ s. Initial concentrations: $[\mathbf{Ox}]_{0,OX} = 0.030$ M, $[H^+]_{0,ACID} = 0.008$ M, $[\mathbf{B}]_{0,both} = 0.014$ M, $[\mathbf{Y}]_{0,both} = 0.01$ M, $w = 1.6$ cm

To investigate the formation of the acidic band, we plot the front positions as the function of time (Fig. 5a and Fig. 5b). At the presence of **Y**, the position of the front defined as the maximums of the derivatives of the [**B**](x) curves (*front B*) separates from the position of the front calculated from the maximums of the derivatives of the pH(x) curves (*front H*). This separation increases with the initial concentration of **Y**. The formation of the main acidic band is due to the excess of **Ox** and the presence of **Y**, which keeps this band localized in the middle. At this zone, **B** is almost completely consumed by the oxidant. *Front H1* is an autocatalytic front which is initiated by the H^+ ions produced at *front B1*, and follows the propagation of *B1* with a delay (Fig. 5b). *Front H1* speeds up as the distance between the two fronts decreases. In the zone between *front H1* and *H1'* there is no remaining B since *front H1* consumes it. This also contributes to the localisation of the main acidic band.

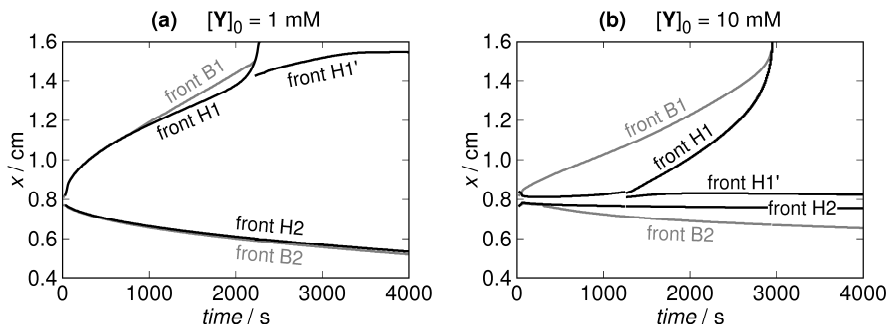**Fig. 5** Temporal evolution of the fronts calculated as the maximums of the derivatives of [**B**](x) curves (*front B*) and pH(x) curves (*front H*) in the presence of different amounts of **Y**. Initial concentrations: [**Ox**]$_{0,OX}$ = 0.030 M, [H$^+$]$_{0,ACID}$ = 0.008 M, [**B**]$_{0,both}$ = 0.014 M, (a) [**Y**]$_{0,both}$ = 0.001 M, (b) [**Y**]$_{0,both}$ = 0.01 M, w = 1.6 cm

In the presence of **Y**, damped oscillation was also found in our one-dimensional simulations. This appears on the time-space plot as thin acidic needles at the beginning of the main acidic band (see Fig. 6). The oscillation cannot be sustained because there is no external reagent supply in this setup. According to our preliminary simulations, the initial separation of **Ox** and H$^+$, and the initial presence of **B** in both sides are essential to oscillation.
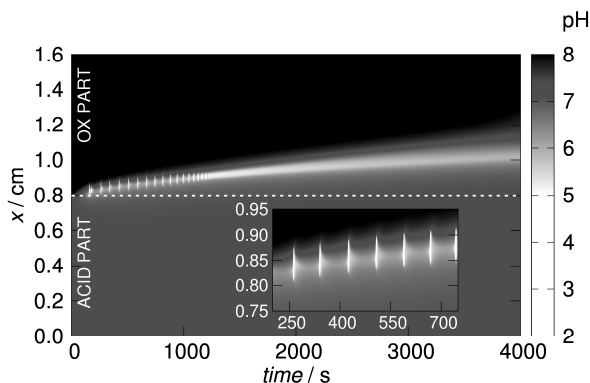

Fig. 6 Calculated spatiotemporal evolution of the damped oscillation. The light colour represents the acidic region. Initial concentrations: [**Ox**]$_{0,OX}$ = 0.019 M, [H$^+$]$_{0,ACID}$ = 0.008 M, [**B**]$_{0,both}$ = 0.014 M, [**Y**]$_{0,both}$ = 0.01 M, w = 1.6 cm

To design experiments where the periodic behaviour can be reproduced, we investigated the properties and significance of the key elements of our kinetic model, which are the autocatalytic steps (R3) and (R4) and the H$^+$-consuming step (R5). Our previous calculations showed that the appearance of oscillations is more sensitive to k_4 than k_3, so we studied the behaviour of our model on the $k_4 - k_5$ parameter plane (Fig. 7). According to these results the domain of the damped oscillation exists only at $k_4 > 10^4$ M^{-1}s^{-1}, which can be assigned only to H$_2$O$_2$ as oxidant. The domain of oscillation is narrow in k_5, which underlines the importance of the kinetics of reaction (R5).
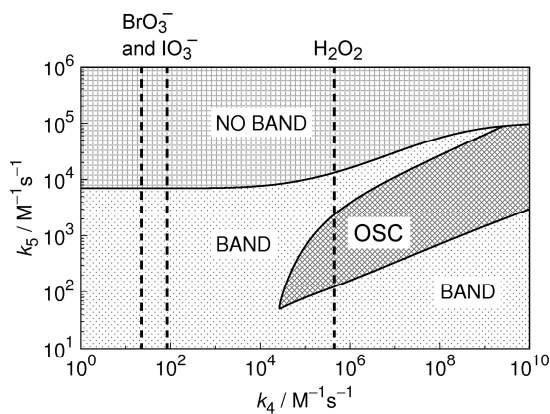
Fig. 7 Calculated phase diagram on the $k_4 - k_5$ plane. The dotted lines indicate the k_4 regimes of different oxidants (bromate, iodate and hydrogen peroxide): $k_{4,\text{bromate}} = 22$ $M^{-1}s^{-1}$ [17], $k_{4,\text{iodate}} = 84$ $M^{-1}s^{-1}$ [estimated value], $k_{4,\text{hydrogen peroxide}} = 2.66 \times 10^5$ $M^{-1}s^{-1}$ [estimated value]. Initial concentrations: $[\mathbf{Ox}]_{0,OX} = 0.019$ M, $[\mathbf{H^+}]_{0,ACID} = 0.008$ M, $[\mathbf{B}]_{0,both} = 0.014$ M, $[\mathbf{Y}]_{0,both} = 0.01$ M, $w = 1.6$ cm

For better understanding of the role of the H^+-consuming step we have modified the stoichiometry and the kinetics of (R5) as it is shown in Table 2, with the corresponding kinetic data. These alternatives correspond to experimentally observed kinetics of H^+-consuming processes used in different pH-oscillators. Besides the original version we have found oscillation only in version (E1). This indicates a significant sensitivity of the oscillatory phenomena to the actual kinetics.

Table 2 Other H^+-consumer steps instead of (R5) of the original model. Stoichiometric and kinetic equations

	stoichiometry		kinetic equations		ref.
E1	$H^+ + \mathbf{Y} + \mathbf{Ox} \rightarrow \mathbf{P_3}$	(e1)	$r_5 = k_5[H^+][\mathbf{Y}][\mathbf{Ox}]$		[18]
			$k_5 = 2.0 \times 10^4$ $M^{-2}s^{-1}$		*this work*
E2	$H^+ + \mathbf{Y} + \mathbf{Ox} \rightarrow \mathbf{P_3}$	(e2)	$r_5 = k_5[\mathbf{Ox}]$		[19]
			$k_5 = 1.6 \times 10^{-4}$ s^{-1}		
E3	$H^+ + \mathbf{Y} \rightleftharpoons \mathbf{P_3}$	(e3)	$r_{51} = k_{51}[H^+][\mathbf{Y}] - k_{51b}[\mathbf{P_3}]$		[20]
			$k_{51} = 9.6 \times 10^4$ $M^{-1}s^{-1}$	$k_{51b} = 4.3 \times 10^{-2}$ s^{-1}	
	$\mathbf{P_3} \rightarrow \mathbf{Q_3}$		$r_{52} = k_{52}[\mathbf{P_3}]$		
			$k_{52} = 3.0 \times 10^{-3}$ s^{-1}		

11

Experimental study

Experimental setup

Two pieces of gels were made of 2 w/w% agarose (Sigma-Aldrich, A2929) with a thickness of $d = 2$ mm. These gels were filled homogeneously with different reactants by soaking them in different stock solutions for one hour, and then the liquid film was wiped off from the gel surfaces. One of the gel pieces, referred as the OX part, contains the oxidant (H_2O_2 or $NaBrO_3$), the other, referred as the ACID part, contains the H_2SO_4, while both parts contain Na_2SO_3, $Na_4[Fe(CN)_6]$ and indicator in equal concentrations. The gel parts were cut to the same size (30 mm × 16 mm (w) × 2 mm) and were put in a covered plastic frame to avoid the contact with oxygen. The setup was thermostated to 25 °C. The gel parts were pushed one against the other by moving and then fixing one side of the plastic frame. The data recording was started when the gel parts got in touch with each other.

The stock solutions were prepared with deionized water. All reactants were used without further purification: H_2O_2 (VWR, 30 % aqueous solution), $NaBrO_3$ (Sigma-Aldrich, ≥ 99 %), Na_2SO_3 (Sigma-Aldrich, Ph. Eur.), $Na_4[Fe(CN)_6] \times 10\ H_2O$ (Sigma-Aldrich, ≥ 99 %), H_2SO_4 (Fluka, volumetric, 1 M), NaOH (Reanal, a.r.), sodium bromocresol purple (Sigma-Aldrich, indicator grade) in case of H_2O_2 and sodium bromocresol green (Sigma-Aldrich, 90 %) in case of $NaBrO_3$. In certain cases, the stock solutions of Na_2SO_3 contain 0.2 mM of NaOH. The initial concentrations were $[Na_2SO_3]_0 = 14$ mM, $[Na_4[Fe(CN)_6]]_0 = 10$ mM, $[\text{bromocresol purple}]_0 = 0.09$ mM or $[\text{bromocresol green}]_0 = 0.21$ mM in both gel parts. The initial concentrations of the oxidant in the OX part and H_2SO_4 in the ACID part were varied.

The pictures were taken by an AVT Stingray F-033B (656×492, 14 bit) camera, and recorded by the Streampix (Norpix) software at a speed of one frame every 20 s. The camera was placed above the experimental setup, which was enlightened by a LED source from beneath. The gels were covered with a 530 nm long-pass filter from both sides to provide better contrast and to protect the ferrocyanide from light. The image processing was made by the ImageJ program.

Results

We have performed experiments with two different oxidants (bromate and hydrogen peroxide) and with different H^+-consuming reactions induced by ferrocyanide, thiourea and hydrogen carbonate. Here, we discuss only the representative hydrogen peroxide-sulfite-ferrocyanide and the bromate-sulfite-ferrocyanide cases. The experimentally observed phenomena are presented as time-space plots, which are drawn from a line perpendicular to the initial interface of the two gel parts. This line is assigned far from the edges to avoid the distortion effect. The experiments are three-dimensional, but the high w/d ratio allows us to draw parallel between the experimental time-space plots and the one-dimensional simulation results.

We carried out experiments at initial concentrations which proved to be successful according to the numerical simulations. Without $[Fe(CN)_6]^{4-}$ an acidic band develops at the contact line of the gel parts after a short initial period. The propagation of the

band is fast and asymmetric in case of both oxidants (Fig. 8a and Fig. 8b). In agreement with our simulation results we could observe the reversal of the front propagation on the ACID side. We tested the dependence of the velocity of the front, which propagates to the direction of the OX part, on the initial concentration of the oxidant. According to the result of the simulations, the experimental velocity of the front become to be almost constant after an initial period. The speed of the front shows a square root dependence on the initial concentration of the hydrogen-peroxide.
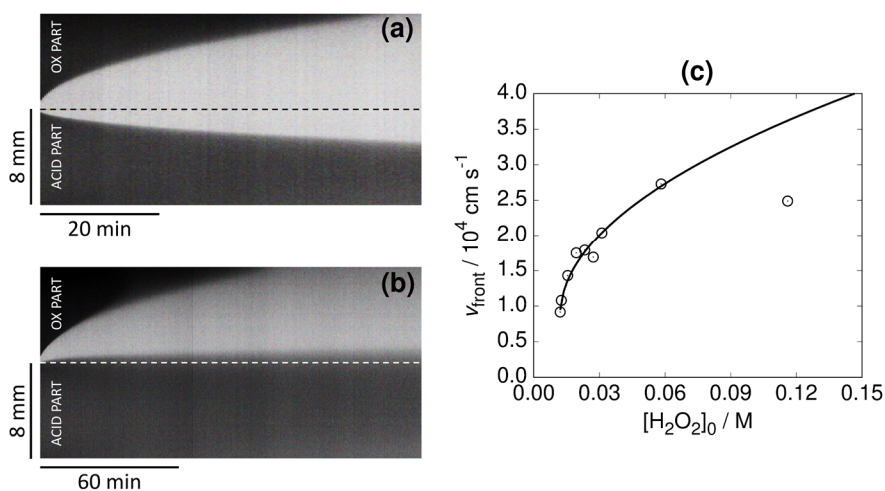

Fig. 8 Experimental results in the absence of the H^+-consuming ferrocyanide in case of H_2O_2 as the oxidant. (a)-(b) Time-space plots of the main acidic band. The light colour represents the acidic region. (c) The dependence of the velocity of the OX-side-front on the initial $[H_2O_2]_0$ concentration. Initial concentrations: (a) $[H_2O_2]_{0,OX} = 0.020$ M, (b) $[H_2O_2]_{0,OX} = 0.013$ M, (a)-(c) $[H^+]_{0,ACID} = 0.008$ M, $[SO_3^{2-}]_{0,both} = 0.014$ M, $[NaOH]_{0,both} = 2 \times 10^{-4}$ M, $w = 1.6$ cm

In the presence of ferrocyanide the acidic band appears, remains thinner compared to the previous case (Fig. 8b). The band shifts to the OX part at a high initial $[SO_3^{2-}]_0 / [\mathbf{Ox}]_0$ ratio and to the opposite direction if this ratio is low, for both oxidants. By using hydrogen peroxide as the oxidant, we could not observe the appearance of acidic arch. Contrary, when bromate ions are applied this phenomenon clearly develops as it is presented in Fig. 9. The recorded lower grayscale intensity at the zone of the arch indicates, that this region is significantly less acidic than the middle one. Although, we have explored wide range of initial concentrations of the reagents and different combinations of the oxidants and the proton consuming processes, we could not obtain spatiotemporal oscillations in the experiments.
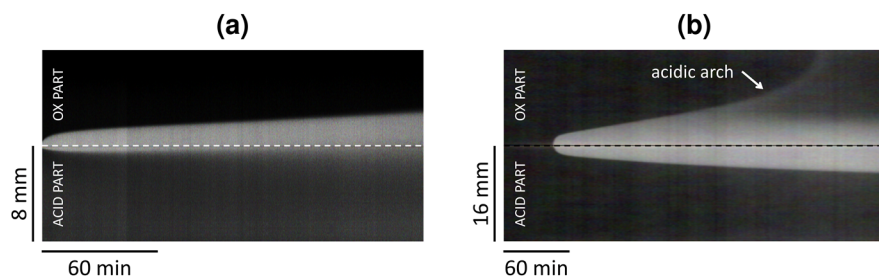
Fig. 9 Experimental time-space plots of the main acidic band and the acidic arch in the presence of the H^+-consuming ferrocyanide in case of (a) H_2O_2 and (b) BrO_3^- as the oxidant. The light colour represents the acidic region. Initial concentrations: (a) $[H_2O_2]_{0,OX} = 0.020$ M, $[H^+]_{0,ACID} = 0.008$ M, $[SO_3^{2-}]_{0,both} = 0.014$ M, $[[Fe(CN)_6]^{4-}]_{0,both} = 0.010$ M, $[NaOH]_{0,both} = 2 \times 10^{-4}$ M, $w = 1.6$ cm, (b) $[BrO_3^-]_{0,OX} = 0.065$ M, $[H^+]_{0,ACID} = 0.030$ M, $[SO_3^{2-}]_{0,both} = 0.080$ M, $[[Fe(CN)_6]^{4-}]_{0,both} = 0.020$ M, $w = 3.2$ cm

14

Discussion and conclusions

In this report, we presented a design strategy to study pattern formation in Landolt-type pH-oscillators with initially separated components. This strategy is potentially applicable for the other types of oscillatory reactions which show oscillations only in the presence of continuous supply of the reagents. These pH-oscillators consists of four initial reagents, an oxidant, the protonated and the unprotonated form of a reductant and a component which induces a hydrogen ion consuming reaction. These chemicals are distributed asymmetrically at the beginning. The mixture of the oxidant with the unprotonated reductant and the hydrogen ion consuming species is on one side. This composition belongs to an unstable state of the system which can be prepared and kept for relatively long period of time, because the rate of the reactions between the components of this mixture are very low. The other part of the system consists of an equilibrium mixture of the protonated and unprotonated form of the reductant and the hydrogen ion consuming species. When these two parts are in contact, the reaction between the oxidant and the protonated reductant takes place at the interface and results in positive feedback for hydrogen ion production. By this type of distribution of the reagents, the key species of the positive feedback (**Ox** and H$^+$) are separated, but the species which provide the negative feedback (**B** and **Y**) are present on both sides.

In the presence of the component which induces the hydrogen ion consuming reaction a separated less acidic zone appears through the bifurcation of the main acidic zone. Contrary to the main zone, which remains close to the interface, this separated zone propagates towards the OX part. This is possible because the rate of the proton consuming process (R5) depends on the actual hydrogen ion concentration. At the neighbourhood of the main zone the rate of (R5) is high enough to slow down effectively the motion of it, which is not the case for the separating less acidic zone.

At some conditions, periodic appearance of the main acidic zone is found in the simulations. The oscillations develop even if the diffusion coefficient of hydrogen ions is set to be equal to the other components (e.g. 1×10^{-5} cm^{2}s^{-1}). Thus, the underlying instability has a kinetic origin. Since in pH-oscillators during an oscillatory cycle one of the main components is nearly totally consumed, the counter diffusion of the components from the two sides is necessary to refill the centre zone with fresh reagents. Contrary to the above discussed front dynamics we could not support this phenomenon experimentally. It is clear from the simulations that the spatiotemporal oscillations can form in a relatively small domain of parameters and are sensitive to the kinetics of the proton consuming step (R5). We believe, that by an appropriate control on the kinetics of the proton consuming process, it would be possible to find this interesting phenomenon in experiments.

Our results show that the dynamics of the A + B $\rightarrow$ C front systems can be significantly enriched by using reactions which include positive and negative feedback processes. Here we presented the transient dynamics of fronts which form at the interface of two compartments loaded with finite amounts of reagents. This configuration naturally results in a continuous change in the concentrations at the outer boundaries. Our preliminary results show, that the use of fixed boundary conditions at the outer boundaries would result in sustained oscillations. This may open a new possibility to study sustained spatiotemporal dynamics of chemical reaction-diffusion systems.

References

1. Zaikin AN, Zhabotinsky AM (1970) Concentration wave propagation in two-dimensional liquid-phase self-oscillating system. Nature 225 (5232):535-537.

2. Tóth Á, Lagzi I, Horváth D (1996) Pattern formation in reaction-diffusion systems: cellular acidity fronts. Journal of Physical Chemistry 100 (36):14837-14839.

3. Müller SC, Ross J (2003) Spatial structure formation in precipitation reactions. Journal of Physical Chemistry A 107 (39):7997-8008.

4. Barge LM, Cardoso SSS, Cartwright JHE, Cooper GJT, Cronin L, De Wit A, Doloboff IJ, Escribano B, Goldstein RE, Haudin F, Jones DEH, Mackay AL, Maselko J, Pagano JJ, Pantaleone J, Russell MJ, Sainz-Díaz CI, Steinbock O, Stone DA, Tanimoto Y, Thomas NL (2015) From chemical gardens to chemobrionics. Chemical Reviews 115 (16):8652-8703.

5. Galfi L, Racz Z (1988) Properties of the reaction front in an A + B → C type reaction-diffusion process. Physical Review A 38 (6):3151-3154.

6. Budroni MA, Lemaigre L, Escala DM, Muñuzuri AP, De Wit A (2016) Spatially Localized Chemical Patterns around an A + B → Oscillator Front. Journal of Physical Chemistry A 120 (6):851-860.

7. Budroni MA, De Wit A (2016) Localized stationary and traveling reaction-diffusion patterns in a two-layer A + B → oscillator system. Physical Review E 93 (6):062207.

8. Budroni MA, De Wit A (2017) Dissipative structures: From reaction-diffusion to chemo-hydrodynamic patterns. Chaos 27:104617.

9. Orbán M, Kurin-Csörgei K, Epstein IR (2015) pH-Regulated Chemical Oscillators. Accounts of Chemical Research 48 (3):593-601.

10. Szalai I, Horváth J, De Kepper P (2015) Contribution to an effective design method for stationary reaction-diffusion patterns. Chaos 25 (6):064311.

11. Rábai G (1998) Modeling and designing of pH-controlled bistability, oscillations, and chaos in a continuous-flow stirred tank reactor. ACH - Models in Chemistry 135 (3):381-392.

12. Szalai I, Kurin-Csörgei K, Orbán M (2012) Modelling pH oscillators in open, semi-batch and batch reactors. Reaction Kinetics, Mechanisms and Catalysis 106 (2):257-266.

13. Virányi Z, Szalai I, Boissonade J, De Kepper P (2007) Sustained spatiotemporal patterns in the bromate-sulfite reaction. Journal of Physical Chemistry A 111 (33):8090-8094.

14. Vanysek P (2003) Ionic conductivity and diffusion at infinite dilution. In: CRC Handbook of Chemistry and Physics. CRC Press, pp 931-933.

15. Liu X, Ramsey MM, Chen X, Koley D, Whiteley M, Bard AJ (2011) Real-time mapping of a hydrogen peroxide concentration profile across a polymicrobial bacterial biofilm using scanning electrochemical microscopy. PNAS 108 (7):2668-2673.

16. Hindmarsh AC, Brown PN, Grant KE, Lee SL, Serban R, Shumaker DE, Woodward CS (2005) SUNDIALS: Suite of nonlinear and differential/algebraic equation solvers. ACM Transactions on Mathematical Software 31 (3):363-396.

17. Kovács K, Leda M, Vanag VK, Epstein IR (2009) Small-amplitude and mixed-mode pH oscillations in the bromate-sulfite-ferrocyanide-aluminum(III) system. Journal of Physical Chemistry A 113 (1):146-156.

18. Edblom EC, Luo Y, Orbán M, Kustin K, Epstein IR (1989) Kinetics and mechanism of the oscillatory bromate-sulfite-ferrocyanide reaction. Journal of Physical Chemistry 93 (7):2722-2727.

19. Rábai G, Kustin K, Epstein IR (1989) A Systematically Designed pH Oscillator: The Hydrogen Peroxide-Sulfite-Ferrocyanide Reaction in a Continuous-Flow Stirred Tank Reactor. Journal of the American Chemical Society 111 (11):3870-3874.

20. Rábai G, Hanazaki I (1996) Chaotic pH oscillations in the sulfur(IV)-hydrogen peroxide-marble flow system. Journal of Physical Chemistry 100 (38):15454-15459.